Study of a contracted glow in low-frequency plasma-jet discharges operating with argon

F. Minotti, L. Giuliani, M. Xaubet, and D. Grondona

Citation: Physics of Plasmas **22**, 113512 (2015); doi: 10.1063/1.4936277
View online: http://dx.doi.org/10.1063/1.4936277
View Table of Contents: http://scitation.aip.org/content/aip/journal/pop/22/11?ver=pdfcov
Published by the AIP Publishing

Study of a contracted glow in low-frequency plasma-jet discharges operating with argon

F. Minotti, L. Giuliani, M. Xaubet, and D. Grondona
Departamento de Física, Facultad de Ciencias Exactas y Naturales, Universidad de Buenos Aires, Buenos Aires, C1428EHA, Buenos Aires, Argentina and Instituto de Física del Plasma (INFIP), Consejo Nacional de Investigaciones Científicas y Técnicas (CONICET), Universidad de Buenos Aires (UBA), C1428EHA, Buenos Aires, Argentina

(Received 24 August 2015; accepted 9 November 2015; published online 25 November 2015)

In this work, we present an experimental and theoretical study of a low frequency, atmospheric plasma-jet discharge in argon. The discharge has the characteristics of a contracted glow with a current channel of submillimeter diameter and a relatively high voltage cathode layer. In order to interpret the measurements, we consider the separate modeling of each region of the discharge: main channel and cathode layer, which must then be properly matched together. The main current channel was modeled, extending a previous work, as similar to an arc in which joule heating is balanced by lateral heat conduction, without thermal equilibrium between electrons and heavy species. The cathode layer model, on the other hand, includes the emission of secondary electrons by ion impact and by additional mechanisms, of which we considered emission due to collision of atoms excited at metastable levels, and field-enhanced thermionic emission (Schottky effect). The comparison of model and experiment indicates that the discharge can be effectively sustained in its contracted form by the secondary electrons emitted by collision of excited argon atoms, whereas thermionic emission is by far insufficient to provide the necessary electrons. © *2015 AIP Publishing LLC*.
[http://dx.doi.org/10.1063/1.4936277]

I. INTRODUCTION

Atmospheric-pressure plasma jets have become the basis of a variety of important applications in plasma medicine and plasma biology.[1,2] For these applications, a crucial aspect is the presence of reactive species, as well as the relatively low temperature of the massive components of the plasma. From a fundamental approach, it is thus very important to understand the physical characteristics and mechanisms of generation of the plasma, in order to better predict the resultant active species, and to properly design the discharge for maximum efficiency.

This kind of discharges can be produced with relatively simple power sources, many commercially available, using configurations of enclosed electrodes that allow the working gas to be blown through them in order to generate an emerging jet.

In this work, we study a plasma jet generated by applying an ac high voltage (about 10 kV) of low frequency (50 Hz) between two disk-shaped electrodes with a hole in the center and separated by a dielectric material. In a previous work,[3] it was found that the *V-I* characteristic of this plasma jet could be explained by an arc-like main channel plus a cathode layer with a large voltage drop (compared to those corresponding to arc discharges). The main channel was modeled using Elenbaas-Heller equation stating the balance between joule heating and radial heat conduction in a cylindrical channel, while a constant cathode drop was added to match the measured values, without any particular modeling, except the justification of its large value by the high collisionality of the ions in the cathode layer.

In the present work, we develop a more detailed model for the cathode layer, including transport, ionization, and recombination of the charged species, and mechanisms for electron emission other than the secondary emission by ion impact, such as field-enhanced thermionic emission and by collision of excited, metastable atoms. Integration of the resulting equations requires the knowledge of the electric field and of the mean electron density in the main channel, obtained from the main channel model, so that both models are matched together, and the *V-I* characteristic and cathode voltage are self-consistently evaluated. Additionally, from electrical diagnostic measurements experimental *V-I* characteristic curves are obtained. Using their dependence on the electrode separation, the electric field in the main channel and the cathode layer voltage are experimentally determined and compared with the theoretical model. Furthermore, estimation of heavy species temperature, obtained from spectroscopic measurements, is also contrasted with that employed in the model.

II. MODEL OF THE DISCHARGE

A. Model of the cathode layer

In order to develop a model of the cathode layer, we consider it as stationary and one dimensional. The stationarity is justified by the relatively low frequency of the discharges studied (50 Hz), much smaller than the relaxation frequencies of the plasma, while the one-dimensionality follows from the expected width of the layer being much smaller than its cross section dimensions, what is a posteriori verified (width up to a few μm and cross section diameter of the main channel above 100 μm). Besides, as the expected layer voltage is relatively large, diffusive flows of charged species can be neglected as compared with field induced

flows. The last assumption can be justified by comparing both flows

$$\frac{j_{mov}}{j_{diff}} \approx \frac{n\mu E}{Ddn/dx} = \frac{neE/T}{dn/dx} \approx \frac{e\Delta V}{T\alpha\Delta x},$$

where Einstein's relation between mobility μ and diffusion coefficient D for each species was used. The species temperature T is given in energy units, n is the species number density, e is the elementary charge, α is Townsend's ionization coefficient, E is the electric field in the layer, Δx its thickness, and ΔV is the potential drop across it. As T is below 1 eV, the expected ΔV above 100 V, and $\alpha\Delta x$ below a few tens, diffusive flows can be neglected. Note that this approximation would not be valid for the cathode layer in an arc discharge in which the potential drop is an order of magnitude smaller.

Using a Cartesian x axis with origin at the cathode surface, the equations for the electron and ion species can be written as

$$\frac{d}{dx}(n_e\mu_e E_x) = -n_e\alpha\mu_e|E_x| + \beta n_e n_i, \tag{1}$$

$$\frac{d}{dx}(n_i\mu_i E_x) = n_e\alpha\mu_e|E_x| - \beta n_e n_i, \tag{2}$$

where α is again Townsend's ionization coefficient, β is the bulk recombination coefficient, and E_x is the x component of the electric field. These equations are complemented with Poisson's equation,

$$\frac{dE_x}{dx} = \frac{e}{\varepsilon_0}(n_i - n_e). \tag{3}$$

Taking the mobilities as constant in the layer, subtracting Eq. (2) from Eq. (1), using Poisson's equation (3), and Eq. (1) again, we obtain (we denote $|E_x| = E$)

$$\frac{d^2}{dx^2}(E^2) = \frac{2e}{\varepsilon_0}(1 + \mu_e/\mu_i)\frac{d}{dx}(n_e E),$$

which on integration yields (neglecting the number one as compared with the ratio of mobilities)

$$\frac{dE}{dx} = \frac{e}{\varepsilon_0}\frac{\mu_e}{\mu_i}\left[n_e - n_\infty\frac{E_\infty}{E}\right], \tag{4}$$

where the boundary conditions $dE/dx = 0$, $n_e = n_\infty$, $E = E_\infty$ were used, as those corresponding to the discharge main channel, obtained from the model described below.

From Eqs. (1) and (4) we derive

$$\frac{1}{n_e}\frac{dn_e}{dx} = \alpha - \frac{1}{E}\frac{dE}{dx} - \frac{\beta n_i}{\mu_e E}. \tag{5}$$

Finally, from Poisson's equation (3) and Eq. (4) we have

$$n_i = n_e - \frac{\mu_e}{\mu_i}\left[n_e - n_\infty\frac{E_\infty}{E}\right]. \tag{6}$$

Defining the dimensionless magnitudes

$$\eta \equiv \frac{n_e}{n_\infty}, \quad \xi \equiv \frac{E_\infty}{E}, \tag{7}$$

Eqs. (4) and (5) are written, respectively, as

$$\frac{d\xi}{dx} = \frac{en_\infty}{\varepsilon_0 E_\infty}\frac{\mu_e}{\mu_i}\xi^2(\xi - \eta), \tag{8}$$

$$\frac{1}{\eta}\frac{d\eta}{dx} = \alpha + \frac{1}{\xi}\frac{d\xi}{dx} - \frac{\beta n_\infty}{\mu_e E_\infty}\xi\left[\eta - \frac{\mu_e}{\mu_i}(\eta - \xi)\right], \tag{9}$$

where Eq. (6) was used to write Eq. (9). By further writing

$$\frac{d\eta}{dx} = \frac{d\eta}{d\xi}\frac{d\xi}{dx},$$

we finally obtain from Eqs. (8) and (9)

$$\frac{1}{\eta}\frac{d\eta}{d\xi} = \frac{1}{\xi} + \frac{\tilde{\alpha}}{\xi^2(\xi - \eta)} - \tilde{\beta}\frac{\eta + (\xi - \eta)\mu_e/\mu_i}{\xi(\xi - \eta)}, \tag{10}$$

where $\tilde{\alpha}$ and $\tilde{\beta}$ are dimensionless ionization and recombination coefficients, respectively, given by

$$\tilde{\alpha} \equiv \alpha L, \quad \tilde{\beta} \equiv \frac{\varepsilon_0}{\mu_e e}\beta, \tag{11}$$

where the constant L, with dimensions of length, is given by

$$L \equiv \frac{\varepsilon_0 E_\infty}{en_\infty}\frac{\mu_i}{\mu_e}. \tag{12}$$

At this point, we consider the boundary conditions at the cathode

$$(n_e\mu_e E)|_{x=0} = \gamma(n_i\mu_i E)|_{x=0} + \phi_0, \tag{13}$$

$$\left.\frac{dn_i}{dx}\right|_{x=0} = 0. \tag{14}$$

Equation (13) represents the emission of electrons from the cathode by ion impact with secondary emission coefficient γ, plus a flow of electrons ϕ_0 due to other mechanisms of emission, such as thermoionic emission or by collision by metastable excited atoms. On the other hand, condition (14) is usually employed[4] to simulate the very thin ion diffusion sublayer, not describable by a fluid model.

Using definitions (7) and the charge continuity relation (derived from the difference of Eqs. (1) and (2))

$$(n_e\mu_e + n_i\mu_i)E = n_\infty\mu_e E_\infty,$$

condition (13) is written as

$$\frac{\eta_0}{\xi_0} = \frac{\gamma}{\gamma + 1}\left[1 + \frac{\phi_0}{\gamma n_\infty\mu_e E_\infty}\right], \tag{15}$$

where ξ_0 and η_0 denote the values of ξ and η, respectively, at $x = 0$.

Evaluation of Eq. (2) at $x = 0$ with condition (14), together with Poisson's equation (3) and relation (13), results in

$$\eta_0\tilde{\alpha}(\xi_0) = \xi_0(\xi_0 - \eta_0)(\xi_0 - \eta_0 + \tilde{\beta}\eta_0), \tag{16}$$

where it was made explicit that the ionization coefficient α depends on the electric field.

In this way, given the electric field E_∞, the electron density n_∞ at the channel, and a value of ϕ_0, relations (15) and (16) allow to determine ξ_0 and η_0. Equation (10) then allows to determine $\eta(\xi)$ in the whole layer $\xi_0 \le \xi \le 1$.

Furthermore, since a voltage increment dV can be written as

$$dV = -E_x dx = Edx = \frac{E_\infty}{\xi}\frac{d\xi}{d\xi/dx},$$

the value of the voltage drop in the cathode layer, ΔV, can be evaluated, using Eq. (8), as

$$\Delta V = E_\infty L \int_{\xi_0}^{1} \frac{d\xi}{\xi^3(\xi-\eta)}. \tag{17}$$

Finally, the spatial variable $x(\xi)$ is obtained, from Eq. (8), by integration of

$$\frac{dx}{d\xi} = \frac{\varepsilon_0 E_\infty}{e n_\infty}\frac{\mu_i}{\mu_e}\frac{1}{\xi^2(\xi-\eta)}$$

with the boundary condition $x(\xi_0) = 0$, so that the cathode layer thickness Δx can be obtained as $x(\xi = 1)$

$$\Delta x = L \int_{\xi_0}^{1} \frac{d\xi}{\xi^2(\xi-\eta)}. \tag{18}$$

1. Modeling different mechanisms of electron emission

In addition to secondary emission by ion impact, electrons can also be emitted from the cathode by thermionic effect, as well as by interaction with atoms or molecules excited at metastable levels. For electric fields at the cathode surface below 5×10^9 V m^{-1}, the emitted electron flow (electrons per second per square meter) by thermionic−Schottky effect can be modeled as[5]

$$\phi_{TE} = \chi\, 1.35 \times 10^{33} T^2 \exp\left[-\frac{\varphi_m - V_E}{T}\right], \tag{19}$$

where T is in eV units, φ_m is the metal work function and $V_E = \sqrt{eE_0/(4\pi\varepsilon_0)}$, with E_0 the electric field at the cathode. The non-dimensional constant χ can take values approximately between 0.125 and 2.5 to account for different surface conditions.[6]

On the other hand, evaluation of the electron emission by impact of metastable atoms requires the knowledge of the flow of these atoms to the cathode and of the corresponding effective secondary emission coefficient γ_m. Following Ref. 7, the equation for the number density distribution of metastable atoms can be written as

$$D_m \frac{d^2 n_m}{dx^2} = -n_e \alpha_m \mu_e E + \frac{n_m}{\tau_m}, \tag{20}$$

where α_m is Townsend's coefficient for atom excitation to the considered level, τ_m is the lifetime of excited atoms, and D_m is their diffusion coefficient. The solution of Eq. (20) not diverging at $x \to \infty$, and with boundary condition $n_m(x=0) = 0$, can be obtained analytically as

$$n_m(x) = \frac{\mu_e}{2}\sqrt{\frac{\tau_m}{D_m}}\left\{2\sinh(k_m x)\int_0^\infty n_e\alpha_m E dx + \int_0^x n_e\alpha_m E\, \exp\left[k_m(x'-x)\right]dx' - \int_0^x n_e\alpha_m E\, \exp\left[k_m(x-x')\right]dx'\right\},$$

where $k_m = 1/\sqrt{D_m\tau_m}$.

The flow of metastable atoms to the cathode can then be expressed as

$$f_m = -D_m \left.\frac{dn_m}{dx}\right|_{x=0} = \mu_e \int_0^\infty n_e\alpha_m E\, \exp(k_m x)dx, \tag{21}$$

and the corresponding flow of emitted electrons as

$$\phi_m = \gamma_m \mu_e \int_0^\infty n_e \alpha_m E\, \exp\left(k_m x\right)dx. \tag{22}$$

Expressions (19) and (22) are possible models for the term ϕ_0 in the boundary condition (13). Note that if relation (22) is employed, it must be self consistently determined along with the solution of Equation (10). In order to do this, Eq. (22) can be more conveniently written using the nondimensional variables (7) and changing the integration variable from x to ξ, using Eq. (8), as

$$\phi_m = \gamma_m n_\infty \mu_e E_\infty L \int_{\xi_0}^{1} \frac{\alpha_m(\xi)\eta}{\xi^3(\xi-\eta)} \exp[k_m x(\xi)]d\xi. \tag{23}$$

B. Model of the main channel

The values n_∞ and E_∞ of the main channel, matching the boundary layer, were determined similarly as in Ref. 3. The main channel is modeled as a non-thermal plasma cylinder of radius R_c in which the Joule heating is balanced by radial thermal conduction at each axial position, which is expressed by the Elenbaas-Heller equation[6]

$$\frac{1}{r}\frac{d}{dr}\left[r\lambda\frac{dT}{dr}\right] + \sigma E_\infty^2 = 0, \tag{24}$$

where $T(r)$ is the electron temperature at each radial position r, and λ and σ are the thermal and electrical conductivities, respectively. For the non-thermal plasma, the conductivities λ and σ are those evaluated for a two temperature plasma, given usually in terms of $T(r)$ and the ratio θ of electron to heavy species temperature.[8] Given a value of R_c and of $T(r=0)$, the electric field E_∞ is determined as the eingenvalue for which $T(r = R_c)$ is near ambient temperature.

As the plasma channel is assumed of uniform, atmospheric pressure, the gas density can be determined from the

heavy species temperature, from which the electron density is determined, using the Saha equation. The value of n_∞ used is then the channel mean electron density weighted by cross-section area, which ensures the continuity of charge between cathode layer and main channel.

The parameters to be determined are the values of R_c and θ. In order to fix these parameters, we explored the set (R_c, θ) able to reproduce both, the value of E_∞ as a function of the discharge current (determined from the measured V-I characteristics for different electrode separations, as detailed below), and the correct magnitude of the heavy species temperature, determined from the spectroscopic measurements.

III. EXPERIMENTAL SETUP

A schematic of the experimental device used to produce the atmospheric plasma jet is shown in Figure 1. This device consists of two electrodes with a hole of 1 mm diameter, through which the gas flows. The two electrodes are made of stainless steel disks of 20 mm diameter and 3 mm thickness attached to the surface of centrally perforated dielectric disks (Teflon) of different thicknesses d. The hole at the center of the dielectric disk is 2 mm in diameter. The ac power supply is a commercially available transformer for neon light (12 kV, 70 mA, and 50 Hz), which is connected to a variable autotransformer (Variac) to control the operating voltage amplitude.

The gas flow was measured using a stainless steel float flow meter. The voltage V between the electrodes was measured using a high voltage probe (Tektronix P6015A, 1000×) connected to a digital oscilloscope (Tektronix TDS2004B, 60 MHz, 1 GS/s), and the current I was inferred from the voltage drop through a 100 Ω resistance (see Figure 1). Different electrode separations d were obtained using dielectric disks of different thicknesses in the range of 1.3–10.2 mm.

The spectroscopic measurements were performed with a monochromator (Diffraction grating: 2400 lines/mm; entrance/exit slit: 170/40 μm) attached to a photomultiplier (Hamamatsu 1P28). The entrance slit was mounted facing the plasma jet, collecting the light emitted not only from the plasma plume but also that from the interelectrode region.

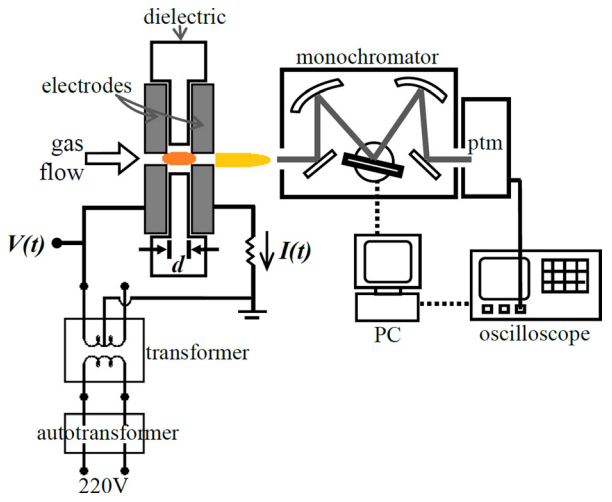

FIG. 1. Experimental device.

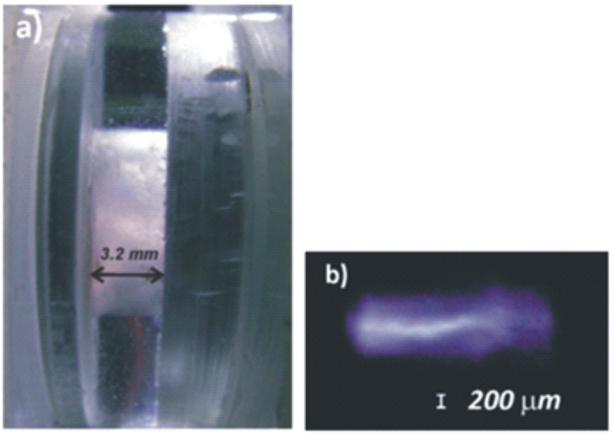

FIG. 2. (a) Long-time exposure photograph of the discharge showing the electrodes. (b) short-time (4 ms) exposure photograph of the discharge showing the contracted channel.

All along this work, the discharge was operated with the power source at its maximum voltage of 12 kV (voltage amplitude at open circuit) and an argon flow of 8 l/min.

In order to observe the discharge, the Teflon disk was replaced by one made of transparent acrylic with a central orifice of 6 mm diameter, shown in Figure 2, together with a detail of the discharge channel.

IV. RESULTS

Typical signals of current and voltage taken during the discharge are shown in Figure 3. The discharge current has a sinusoidal profile with a frequency of 50 Hz, almost independent of the discharge characteristics, since it is controlled by the transformer impedance. The displacement current, measured with the discharge off, is negligible compared with the discharge current. The voltage signal also has a frequency of 50 Hz and decreases when the current increases and vice versa. This behavior results in a negative slope in the V-I characteristic of the discharge.

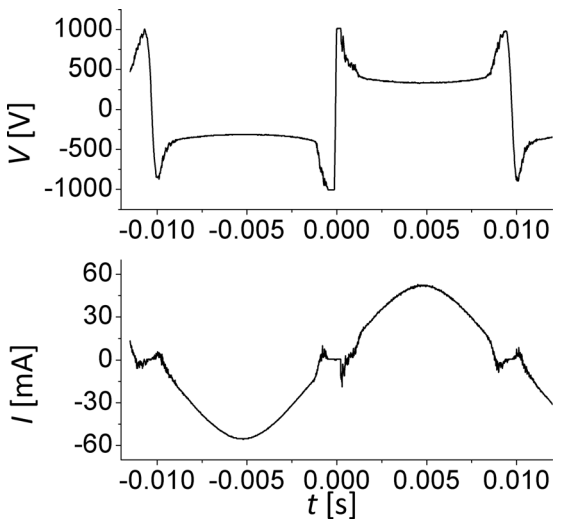

FIG. 3. Voltage and current signals of the jet for $d = 7$ mm.

The experimental main channel electric field $E_\infty(I)$ as a function of the current I was determined from the measured characteristics as

$$E_\infty(I) = \frac{V_i(I) - \Delta V(I)}{d_i}, \tag{25}$$

where the subscript i denotes an electrode separation and ΔV is the voltage in the cathode layer, assumed to be independent of d_i (but dependent on the discharge current), in such a way that if "1" and "2" denote two different separations, one can write that

$$E_\infty(I) = \frac{V_2(I) - \Delta V(I)}{d_2} = \frac{V_1(I) - \Delta V(I)}{d_1},$$

where the cathode layer thickness was neglected as compared with the electrode separation (the model predicts layer thickness of a few μm). In this way, the cathode voltage can be determined as

$$\Delta V(I) = \frac{d_2 V_1(I) - d_1 V_2(I)}{d_2 - d_1}. \tag{26}$$

Figure 4 shows the experimental cathode voltage obtained using $d_2 = 10.2$ mm and $d_1 = 1.3$ mm, which are the longest and shortest electrode separations, respectively. Using the experimental values of $\Delta V(I)$, the main channel electric field was obtained from Eq. (25), and shown in Figure 5 for $d = 10.2$ mm. In the same figure, the modeled electric field $E^m_\infty(I)$ predicted by the non-thermal plasma model for the main channel is also shown, corresponding to a channel radius $R_c = 100\,\mu$m and $\theta = 5.5$, 6, and 6.5, together with the case $R_c = 140\,\mu$m, $\theta = 5.5$, included for comparison. This last case corresponded to the largest radius for which solutions similar to the experimental ones for some θ are possible. Values of θ larger than those presented did not result in correct electric field values for any R_c, while lower values were inconsistent with the measured low temperature of heavy species.

For the range of currents in the experiment (10–70 mA), a radius of the channel $R_c = 100\,\mu$m leads to current densities in the range of 30–220 A cm^{-2}. Electron temperatures at the axis range from about 7300 K for 10 mA to 9000 K for 70 mA. The corresponding heavy species temperature for $\theta = 6$ are then in the range of 1200–1500 K, similar to those obtained from the spectroscopic measurement (see below).

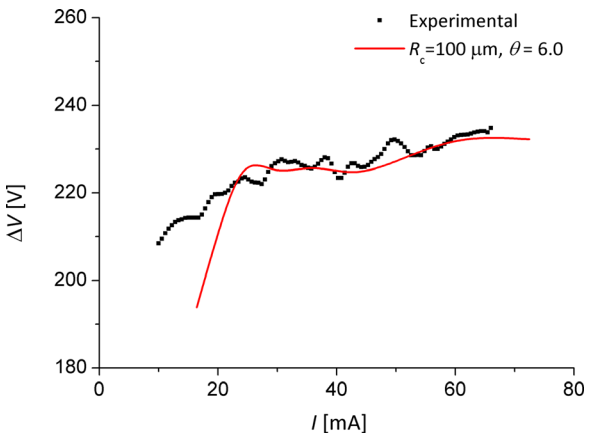

FIG. 4. Cathode-layer voltage as a function of the discharge current. Dots: experimental values, lines: theoretical cathode voltage for plasma conditions in the main channel determined from the main-channel model with $R_c = 100\,\mu$m and $\theta = 6$.

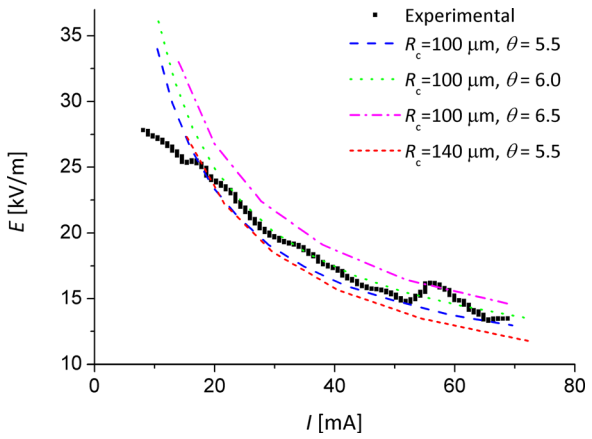

FIG. 5. Main-channel electric field as a function of the discharge current. Squares: Experimental value corresponding to an electrode separation $d = 10.2$ mm. Lines: theoretical model for different values of channel radius R_c, and of ratio of electron to heavy species temperatures θ.

In order to model the cathode layer, the secondary electron emission coefficient was taken $\gamma = 0.05$, as indicated by the best fit to different abnormal glow discharges in argon.[9] Expressions of the ionization Townsend's coefficient as a function of the electric field and of the dissociative recombination coefficient as a function of the electron temperature were taken from Chapter 4 of Ref. 6 and from Ref. 10. Townsend's coefficient for molecule excitation to metastable level Ar(^{3}P$_2$) was taken as that for ionization,[11] corrected for the difference between ionization and excitation energies. Concerning the metastable lifetime, for small extension of the cathode layer (below 10 μm), the results are not sensitive to lifetime values above 1 μs because the exponential inside the integral in Eq. (23) is essentially of value one.

In Figure 4, it is included the modeled cathode voltage values $\Delta V_m(I)$ calculated with the cathode layer model, Eq. (17), using the $E^m_\infty(I)$ and $n_\infty(I)$ obtained from the non-thermal channel model with $R_c = 100\,\mu$m, $\theta = 6.0$. It can be seen that values of the cathode voltage are around 220 V, well fitting the experimental values, and also similar to those observed in abnormal glow discharges in argon.[9] The corresponding layer thickness obtained from the model, Eq. (18), is about $1-3\,\mu$m for the range of currents of the experiment. Using Eq. (19) to model thermionic emission, it was verified that with cathode temperatures as high as 1500 K, about the melting point of the cathode material (steel), this mechanism was insufficient by one to two orders of magnitude to supply the electron flow necessary to sustain a discharge with the measured cathode voltages. On the other hand, secondary emission by collision of metastable atoms Ar(^{3}P$_2$) provided an electron flow, according to Eq. (23), which led to a $\Delta V_m(I)$ similar to the measured one, using $\gamma_m = 0.4 - 0.7$. Since reported values of this coefficient are very high,[12] $\gamma_m \approx 1$, we see that sustainment of the discharge can be

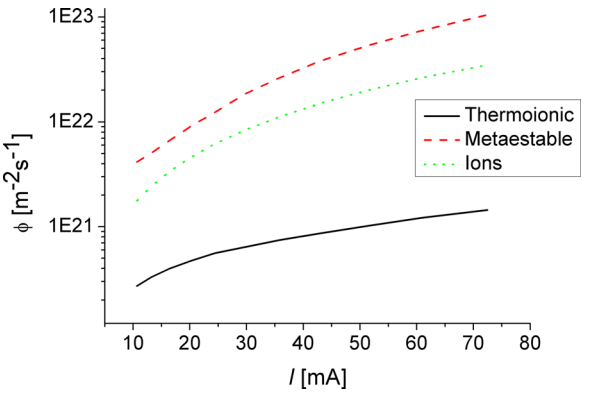

FIG. 6. Modeled electron flow from the cathode for the three considered mechanisms (secondary electron emission by ions, thermionic emission, and electron emission by collision of metastable atoms).

consistently explained in this way. The relative importance of the three considered mechanisms of electron emission from the cathode can be appreciated in Figure 6. In this figure, the modeled electron flow from the cathode for $R_c = 100\,\mu$m and $\theta = 6.0$ as a function of the discharge current are calculated for secondary emission by ions, thermionic emission and secondary emission by collision of metastable atoms.

Finally, the *V-I* characteristics were modeled as $V_m(I) = \Delta V_m(I) + E^m_\infty(I)d$, using the modeled values $\Delta V_m(I)$ and $E^m_\infty(I)$ for the case $R_c = 100\,\mu$m, $\theta = 6.0$, and included with the measured characteristics in Figure 7.

As can be seen in Figures 4–7, the modeled magnitudes show a good agreement with the corresponding experimental values only for discharge currents above 20 mA. This problem can be traced to the main channel model which, as shown in Figure 5, predicts excessively large values of $E^m_\infty(I)$ for currents below 20 mA, possibly due to uncertainties in the modeled conductivities at low electron temperatures. An additional consistency check was made analyzing the emission spectra of the plasma, which can be seen in Figure 8, were all remarkable emissions monitored within the 300–440 nm range have been identified.[13,14] It is found that the spectrum shows emissions of molecular nitrogen containing N_2 second positive systems, and peaks

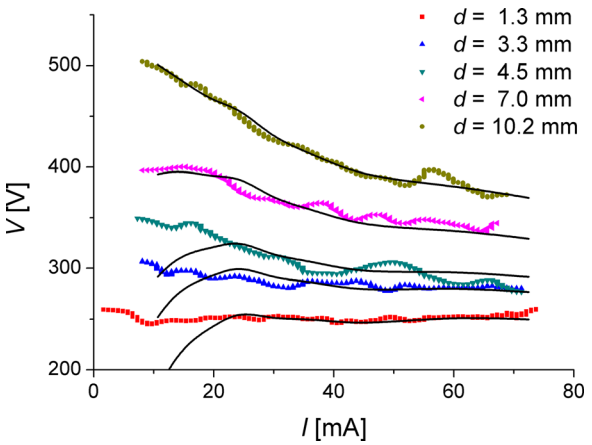

FIG. 7. Experimental (dots) and theoretical (lines) *V-I* characteristics for argon with different electrode separations.

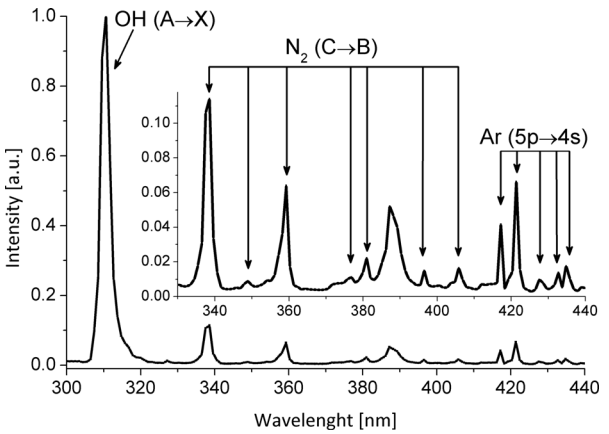

FIG. 8. Emission spectrum of the plasma jet with all remarkable emissions monitored within the 300–440 nm range for argon.

corresponding to OH and Ar. These excited molecules and energetic UV photons play important roles in the sterilizing properties of plasmas.

An experimental spectrum of the 357.7 nm peak of the N_2 2nd positive system (dots + lines) and SPECAIR software spectral simulations (lines) are shown in Figure 9. It was found that the best fits are obtained with rotational temperatures T_r between the values 1200 K and 1500 K, consistent with those of the heavy species obtained from the channel model.

V. CONCLUSIONS

In this work, a model of a low frequency plasma jet discharge was developed and contrasted with experimental results. It was found that a simple model of the main channel as a non-thermal plasma, and a cathode layer model with different mechanisms of electron emission, collisions of argon ions, and argon metastable atoms, reproduced well the measured electric fields and the *V-I* characteristic curves for currents above 20 mA.

In the experiments, we have observed that the discharge has the visual characteristics of a thin, contracted column, which must sustain relatively high current densities. Results from the models employed (and from the observed size of

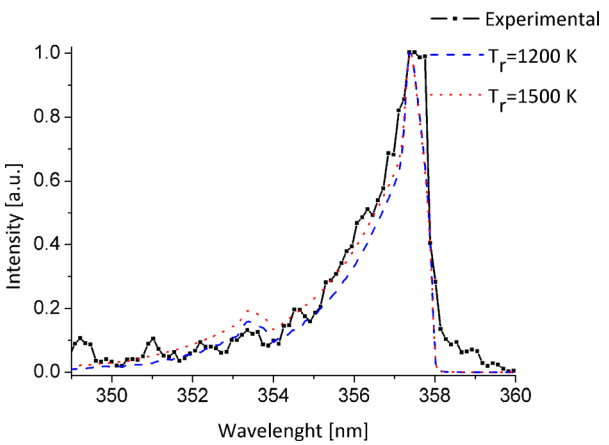

FIG. 9. Experimental spectra of the 357.7 nm peak (dots + lines) and SPECAIR software spectral simulations (lines).

the discharge channel) indicate current densities of similar value (over 100 A cm^{-2}) to those of abnormal glow discharges in argon at atmospheric pressure with similar cathode voltages.[9] A possible scenario for the development of this kind of contracted abnormal glow discharge is the following. Before gas breakdown, a relatively large amount of charge can be accumulated on the electrodes, given the large voltages and the relative proximity and large area of the electrodes, so that when the breakdown takes place, either by streamers or Townsend mechanism (the values of pressure times electrode separation, *pd*, in the device can correspond to either[6]), a high current, spark-like discharge is initiated. Considering now a generic voltage-current (*V-I*) characteristic, the discharge initiates on the high-current region of the characteristic, corresponding to an arc, and as the power source current limitation operates the discharge moves toward the abnormal glow region of the characteristic, thus allowing this type of discharge to be reached from the arc region. At this point, efficient electron generation at the cathode can be achieved by diverse mechanisms to sustain the discharge. In particular, the cathode layer model indicates that mechanisms additional to secondary emission by ion impact are required, as even the highest reported values of the secondary emission coefficient for this process are insufficient to provide the necessary current densities. As it turns out, current densities by thermionic emission, even aided by the electric field, are also insufficient by about two orders of magnitude, while the model predicts a consistently evaluated flow of metastable argon atoms to the cathode, capable of generating enough secondary electrons to sustain the discharge, with values of the corresponding secondary emission coefficient similar to those reported.

Finally, as an example of further information that can be obtained from the model, we briefly consider the derivation of reaction rates k of interest for electron impact processes. For instance, generation of hydroxyl radicals OH are of prime importance in biological applications of plasma jets. From the values of the cross section as a function of the electron energy, $\sigma_{OH}(\varepsilon)$, for the production of OH from water molecules by electron impact,[15] and the distribution function of electron energy, $F(\varepsilon)$, obtained with the Bolsig software,[16] using the neutral number density and electric field strength in the main channel given by the model, the reaction rate for the process can be evaluated as

$$k_{OH} = \sqrt{2e/m}\int_o^\infty F(\varepsilon)\sigma_{OH}(\varepsilon)\varepsilon d\varepsilon,$$

where e and m are the electron charge and mass, respectively. Characteristic values are so obtained to be $k_{OH} \approx 7\times10^{-20}$ m^3 s^{-1} for the employed discharge. On the other hand, production of OH by collision of excited, metastable argon atoms with water molecules is considered of importance given its relatively large cross section[17] $\sigma \approx 6\times10^{-19}$ m^2 (rate reactions of about[18] 2×10^{-16} m^3 s^{-1}). However, this mechanism is expected to exist only in the μm thin cathode layer, because the values of the electric field in the main channel of the argon discharge correspond to negligible values of the Townsend excitation coefficient for argon atoms in this region, so that Eq. (20) predicts negligible excited argon population. Taking as an estimation of the flux of metastable argon atoms that evaluated at the cathode, given by Eq. (21), we obtain a corresponding efficiency of about 10^3 times that of electron impact alone in argon. As electron impact production of OH radicals acts in the mm long channels, both mechanisms can in principle be of similar importance in this discharge.

ACKNOWLEDGMENTS

This work was financed by grants from CONICET: PIP GI 11220120100453, ANPCyT: PICT 2010-0771, and from the University of Buenos Aires: UBACyT 20020130100699BA.

[1]D. B. Graves, Phys. Plasmas **21**, 080901 (2014).
[2]M. G. Kong, G. Morfill, and W. Stolz, in *Plasma Medicine*, edited by M. Laroussi (Cambridge University Press, Cambridge, 2012).
[3]L. Giuliani, M. Xaubet, D. Grondona, F. Minotti, and H. Kelly, Phys. Plasmas **20**, 063505 (2013).
[4]J. P. Boeuf and L. C. Pitchford, Phys. Rev. E **51**, 1376 (1995).
[5]E. L. Murphy and R. H. Good, Phys. Rev. **102**, 1464 (1956).
[6]Y. P. Raizer, in *Gas Discharge Physics*, edited by J. E. Allen (Springer Verlag, Berlin, 1991), pp. 68–71, 277, and 327.
[7]Y. Akishev, V. Karalnik, I. Kochetov, A. Napartovich, and N. Trushkin, Plasma Sources Sci. Technol. **23**, 054013 (2014).
[8]M. I. Boulos, P. Fauchais, and E. Pfender, *Thermal Plasmas: Fundamentals and Applications* (Plenum Press, New York, 1994), Vol. 1, pp. 314–317.
[9]A. V. Phelps, Plasma Sources Sci. Technol. **10**, 329 (2001).
[10]P. Lukáč, O. Mikuš, I. Morva, Z. Zábudlá, J. Trnovec, and M. Morvová, Plasma Sources Sci. Technol. **20**, 055012 (2011).
[11]M. Nikolić, J. Newton, C. I. Sukenik, L. Vušković, and S. Popović, J. Appl. Phys. **117**, 023304 (2015).
[12]F. B. Dunning, A. C. H. Smith, and R. F. Stebbings, J. Phys. B: At. Mol. Phys. **4**, 1683 (1971).
[13]See http://www.nist.gov/pml/data/asd.cfm for NIST atomic database.
[14]R. Pearse and A. Gaydon, *The Identification of Molecular Spectra* (John Wiley & Sons, New York, 1941), pp. 137–160.
[15]Y. Itikawaa and N. Mason, J. Phys. Chem. Ref. Data **34**, 1 (2005).
[16]G. J. M. Hagelaar and L. C. Pitchford, Plasma Sources Sci. Technol. **14**, 722 (2005).
[17]H. L. Snyder, B. T. Smith, T. P. Parr, and R. M. Martin, Chem. Phys. **65**, 397 (1982).
[18]H. Sekiya and Y. Nishimura, Chem. Phys. Lett. **171**, 291 (1990).